In-situ n-doped 3D-printed abiotic cathodes for implantable biofuel cells

M. Ghodhbane, D. Beneventi, L. Dubois, A. Zebda, D. Chaussy, N. Belgacem

In-situ n-doped 3D printed abiotic cathodes for implantable biofuel cells

M. Ghodhbane,[a,b] D. Beneventi,[a,*] L. Dubois, [c] A. Zebda,[b] D. Chaussy,[a] N. Belgacem,[a]

[a.] *Univ. Grenoble Alpes, CNRS, Grenoble INP*, LGP2, 38000 Grenoble, France. *Institute of Engineering Univ. Grenoble Alpes.*

[b.] *Univ. Grenoble Alpes, CNRS, UMR 5525, VetAgro Sup, Grenoble INP, INSERM, TIMC, 38000 Grenoble, France.*

[c.] *Univ. Grenoble Alpes, CEA, CNRS, Grenoble-INP, SyMMES, UMR 5819, Grenoble, 38000, France.*

[*] Corresponding author: davide.beneventi@pagora.grenoble-inp.fr

Abstract

Abiotic 3D printed cathodes for biofuel cells were manufactured using chitosan-cellulose nanofibres-iron doped graphene hydrogels and the cold material extrusion (MEX) 3D printing technique. The subsequent pyrolysis under ammoniac flux and in situ n-doping of 3D cathodes led to the generation of conductive 3D electrodes with macroporosity that can be tuned by adjusting the linerar infill in the 3D printing process and enhanced electrochemical activity. In situ n-doped electrodes with 40% macroporosity provided a neat increase in specific current, i.e. from 13 µA/mg of 3D electrodes containing pre-doped graphene to 35 µA/mg of pyrolyzed ones, thus showing that MEX 3D printing followed by in-situ N doping is a promising manufacturing process for the fabrication of high current density abiotic cathodes.

Graphical abstract

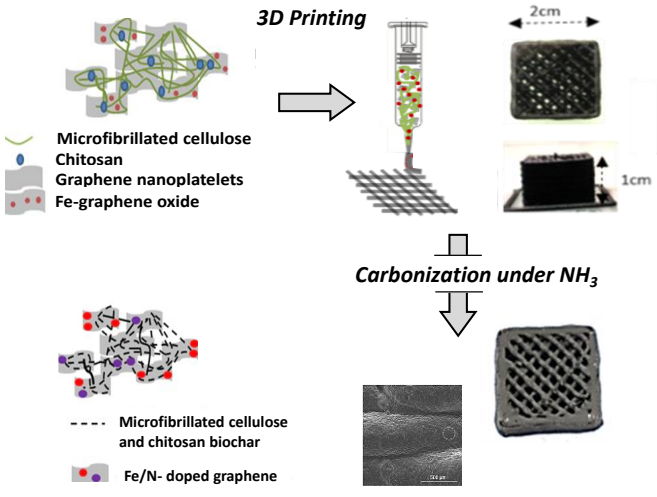

Keywords: abiotic cathodes, biofuel cells, 3D printing, pyrolysis

1 Introduction

Over the last decade, additive manufacturing progressively found application in the field of energy storage paving the way to the production of complex 3D architectures and highly porous electrodes. This method, and in particular cold material extrusion (MEX) coupled with the formulation of viscous functional inks, has been used for the fabrication of a wide variety of electrochemical devices such as lithium-ion batteries [1-4], supercapacitors [5-8], and glucose biosensors [9]. Ink formulation for electrodes manufacturing relies on the combined use of conductive fillers and polymers playing the role of rheology modifier and binder [10], respectively. To this purpose, conductive carbon materials such as carbon nanotubes,11 reduced graphene oxide [12], carbon [6], have been often combined with polymers such as cellulose nanofibrils [2], Pluronic® F127 [4], hydroxypropyl methylcellulose [13] or silica gel [9]. Different manufacturing methods have been adopted varying from simple two-step methods, characterized by ink manufacturing and 3D printing [1,3-8], to methods requiring additional steps after printing such as chemical or thermal reduction [13,14], lyophilization [14,15,16], electrodeposition [4,13]. The fabrication of 3D-printed abiotic cathodes for implantable glucose biofuel cells has been explored only in a recent work [17] showing that a neat increase in electrochemical activity (i.e. 3.6-fold increase in specific current) can be obtained when shifting from 2D compact electrodes to 3D printed macroporous electrodes. This gain was ascribed a better control of the hierarchical porosity (from nano to macroscale) allowing an enhanced diffusion of the chemicals inside 3D electrodes, resulting in a higher accessibility of n-doped graphene active sites. This work was aimed at further increasing the electrochemical activity of abiotic cathodes by 3D printing and in-situ n-doping by pyrolysis under ammoniac flux of the 3D printed electrodes manufactured using Fe-graphene oxide precursors (Fe-GO), graphene nanoplatelets and bio-sourced binders, i.e. chitosan and TEMPO (2,2,6,6-Tetramethylpiperidine-1-oxyl radical)-oxidized cellulose nanofibers (TOCNF). This 3D printing ink formulation was labelled as undoped formulation and compared to a not pyrolyzed formulation containing n-doped graphene (n-doped).

2 Materials and Methods

2.1 Materials

Chitosan and genipin (≥ 98%) were supplied by Sigma Aldrich, graphene nanoplatelet aggregates (06-0235, nominal diameter <2 µm, C content > 99.5%) by Strem Chemicals and TEMPO-oxidized Cellulose Nanofibres (TOCNF) by CTP (Centre Technique du Papier, Grenoble) [18]. MFC were produced from bleached and TEMPO-oxidized hardwood fibres using a sequence of refining and high-pressure homogenization (2 passes at 1500 bars) in order to get a gel-like aqueous suspension with 2% w/w mass fraction of cellulose. In order to obtain iron doped graphene oxide (Fe-GO), commercial graphene nanoplatelets were first treated in a concentrated sulphuric acid/H_2O_2 mixture at 200°C in order to increase porosity and create oxygenated coordination sites (carboxylic acid etc…) for iron(III) ions. After careful washing to remove any trace of acidity, a solution of iron(III) chloride was added and the

mixture was lyophilized in order to obtain 2% w/w Fe-GO precursor. This precursor was both i) formulated with commercial graphene nanoplatelets and biosourced binders (i.e. chitosan and TOCNF) to obtain an ink containing undoped graphene and ii) submitted to heat treatment under ammoniac flux in order to obtain Iron (2%)/Nitrogen doped graphene (Fe/n-G) [19,20].

2.2 Hydrogel formulation

According to a previous work focusing on the optimization of hydrogel formulation for cathodes 3D printing [17], two formulations were prepared by mixing 0.2 g of chitosan, 1 mg of genipin crosslinker and 15 g of TOCNF aqueous suspension with 2% w/w cellulose content with i) 1.88 g of graphene nanoplatelet and 0.62 g of Fe-GO ii) 1.9 g of graphene nanoplatelet and 0.62 g of Fe/n-G. Those formulations were labeled as undoped and n-doped, respectively. For better homogenization and aggregates break up, the prepared inks were processed on a three-rolls mill (5 rpm and rolls gap 1 µm) until getting a hydrogel with a shiny aspect. Samples composition is given in Table 1. Hydrogels were stored in a refrigerator at 6°C and heated at room temperature before use.

The thermogravimetric analysis (TGA) of each material used for ink formulation and of the undoped sample dry formulation was performed under nitrogen flow (40 mL/min) with TGA-DSC3+ Mettler Toledo. The samples were heated at 5 °C/min from room temperature to 150°C (heating rate 5°C/min) and after 30 min dwell at 150°C the temperature was further increased to 400°C (heating rate 0.5°C/min, and 10 min dwell) and 700°C (heating rate 0.5°C/min and 10 min dwell).

Table 1 Composition of the different prepared formulations expressed as total dry solids content in the aqueous paste and weight fractions of the dry solids. Owing to the extremely low mass used for electrodes formulation, genipin was omitted

Sample	Dry solids content (%)	Water content (%)	Chitosan (%)	TOCNF (%)	Graphene (%)
Undoped	16.9	83.1	6.6	10	83.3 (1/4 Iron 2% doped graphene)
n-doped	16.9	83.1	6.6	10	83.3 (1/4 Nitrogen, Iron 2 % doped graphene)

2.3 3D electrodes manufacturing and characterization

3D cathodes were printed using a cold material extrusion 3D printer (3D Culture) equipped with a piston extrusion system. The two ink formulations were used to print 2×2×1 cm^3 cuboids at room temperature using a nozzle of 0.96 mm diameter and a speed of 5 mm/s. The layer height was set to 0.6 mm, the linear infill was set to 30, 40, 50 and 100% and cathodes were printed using a unit perimeter layer without top/bottom layers. The printed cathodes were air dried at room temperature. 3D printed abiotic cathode was synthesised following a simple thermal treatment in order to maximize n-doping while developing the electric conductivity of pyrolyzed cellulose/chitosan [20-22].

After 3D printing, the solid was heated at 700°C for 2 h under an ammonia atmosphere then washed in a 0.5M sulphuric acid solution at 80°C (in order to remove any iron or iron oxide articles) to obtain 3D printed iron-nitrogen doped electrodes. For comparison, Fe-GO was directly pyrolysed under ammonia at 700°C for 2 hours and carefully washed with 0.5M sulphuric acid at 80°C to obtain Fe/n-

G. The morphological properties of the 3D printed electrodes were determined using scanning electron microscopy (ESEM, FEI-Quanta 2000) equipped with EDX Unit device (Energy Dispersive-Xray Analyses).

Nitrogen adsorption-desorption isotherms were measured on a surface area analyzer NOVAtouch™ 2 (Quantachrome Instruments) at 77K. Before the measurements all samples were degassed under vacuum at 40°C for 12 h. Based on the obtained data, samples' specific surface areas (SSA) were calculated using the Brunauer–Emmett–Teller (BET) linear equation in the approximate relative pressure range from 0.1 to 0.3. The correlation coefficient of the linear regression was not less than 0.999. The total pore volume was calculated from the volume adsorbed at p/p_0~0.99.

The electrochemical characterizations were performed using a three-electrode electrochemical cell associated with a Biologic Potentiostat SP150. The 3D printed biocathode was glued to a conductive teflonated gas diffusion layer (H23, Freudenberg) using a carbon-based conductive paste (Loctite EDAG) and used as a working electrode. A platinum electrode was used as a counter electrode and a saturated calomel electrode (SCE) as a reference electrode.

The 3D printed abiotic biocathodes were tested at ambient temperature (20 ± 3°C) in a pH 7.4 physiological medium, i.e. 100 mL of a solution containing phosphate buffer (0.01 mol L^{-1}), NaCl (0.14 mol L^{-1}), KCl (0.0027 mol L^{-1}). The chronoamperometric response of the biocathode was recorded at 0.1 V vs. SCE for 24h under air and saturated oxygen.

3 Results and discussion

The thermogravimetric analysis of the different graphene species used in this study, ie. commercial graphene nanoplatelets, Fe/n-G, and Fe-GO illustrated in Figure 1 shows two regions. A first region, up to 100°C, indicating an initial mass loss of 6—8%, which was associated with the moisture content of the sample, and a second region up to 700°C where samples undergo a constant mass loss owing to a low content of oxygenated group and a high degree of graphene reduction [23].

At 700°C, graphene nanoplatelets and Fe/n-G have a significant residue of ca. 83% whereas, the lower residue of Fe-GO (i.e. 75%) was ascribed to the presence of a higher initial oxygen content. TOCNF displayed the typical cellulose mass loss profile [26], namely a 10% mass loss up to 100°C due to water removal, a plateau up to 220°C and a sharp mass drop of 50% up to ca. 350°C, which is mainly due to cellulose decomposition.

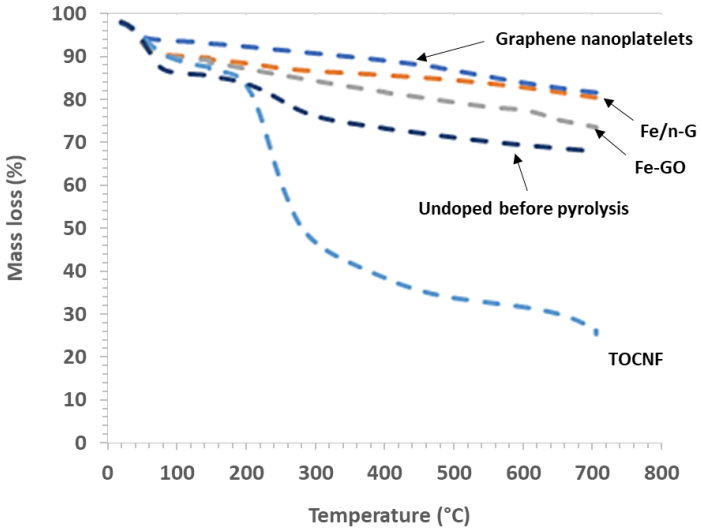

Fig. 1 Thermogravimetric analysis of the different materials used in the ink formulation and the 3D printing formulation before pyrolysis

At 700°C the TOCNF sample had a residual mass of 26%. The air-dried non pyrolyzed formulation shows 14% mass loss at 100°C indicating a higher residual water content, which was associated to water segregation in the crosslinked chitosan/TOCNF network. Then, TOCNF and chitosan degradation between 220 and 350°C and the progressive graphene oxygenated moieties reduction led to a final yield of 68% at 700°C. This value agrees with both: i) the theoretical yield calculated using the formulation composition and the residue of each component, i.e. 70.6%, and it was interpreted as reflecting the absence of any synergy among components during the pyrolysis process and ii) the residues obtained after pyrolysis under N_2 and ammoniac of 3D printed objects, which ranged between 60 and 70% (as determined by sample weighing before and after pyrolysis).

During air drying, 3D printed cuboids (2x2x1 cm^3) with different infill were subjected to: an isotropic shrinkage in the XY plane of 44 ± 4% and a 31 ± 2% shrinkage in the Z direction, respectively. This significant dimensional variation was associated with the low concentration of the pristine hydrogel (16.2%) and its collapse during drying. Figure 2 shows that the pyrolysis step did not induce further shrinkage owing to the high carbon yield of the formulation. Nevertheless, samples with an infill ratio lower than 40% displayed an extremely brittle behaviour, which was not compatible with their use as biocathodes.

SEM analysis of 3D printed samples surface before and after pyrolysis (Figure 2c and d) shows the presence of an extremely rough surface and globular aggregates with sizes ranging between 5-8 µm, which were not observed after pyrolysis. Owing to the presence of random pores with similar size on pyrolyzed samples and the nominal size of graphene aggregates <2 µm, globular aggregates were associated to cellulose and chitosan, which acted as pore templates upon thermal degradation. Nitrogen adsorption-desorption isotherms (Figure 3) on the doped and undoped-pyrolyzed 3D electrode show a type I shape with a hysteresis of type H3 (according to IUPAC classification).

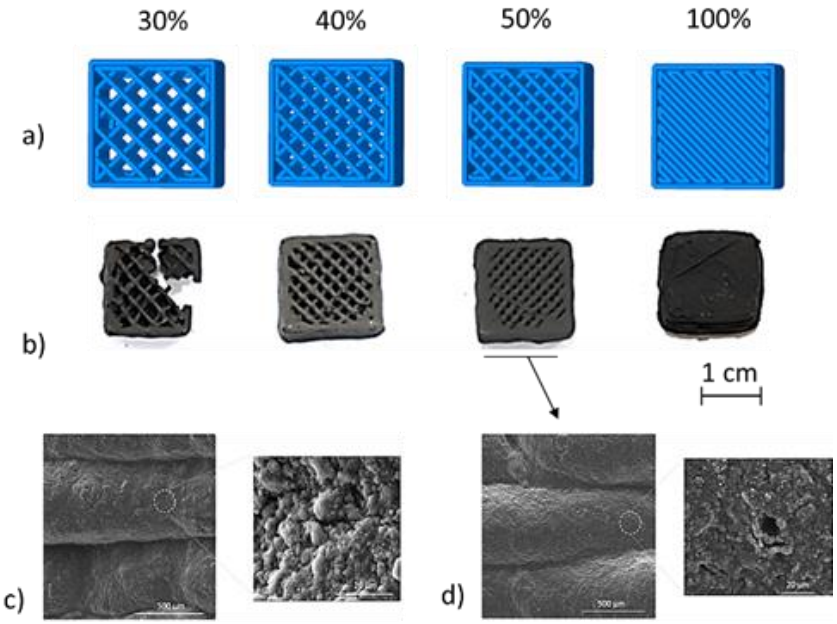

Fig. 2 Pyrolyzed 3D cathodes with different infill ratios, model cubes a) and 3D printed electrodes b). SEM images of filaments surface before c) and after pyrolysis d)

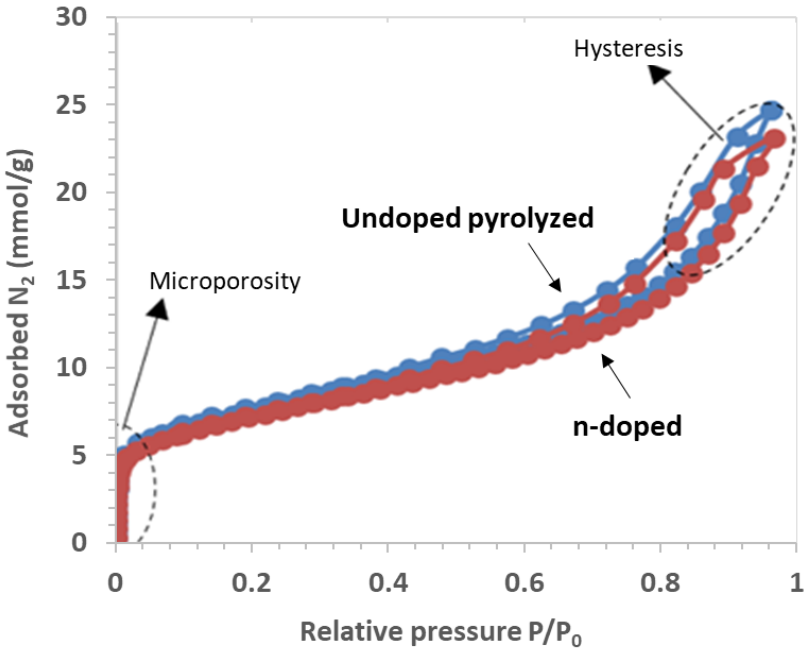

Fig. 3 Nitrogen adsorption/desorption isotherms on doped and undoped-pyrolyzed 3D printed cathodes (77K)

Table 2 Specific surface area and pore volume of graphene nanoparticles and 3D printed cathodes with 40% infill

	S_{BET} (m^2/g)	Micropores vol (cm^3/g)	Total vol (cm^3/g)
n-doped	560	0.1147	0.654
Undoped pyrolyzed	596	0.1187	0.696
Fe/n-G	593	//	0.84
Graphene nanoplatelets	748	//	1.3

The presence of this type of hysteresis was associated to a phenomenon of capillary condensation into graphene aggregates pores [24]. Mesoporosity was excluded since there was no saturation at P/P0 > 0.9 (as for type IV isotherms showing the presence of mesopores). According to the HK method [25], pores had an average size of 0.7 and 0.88 nm showing significant microporosity. In line with ESEM analysis, pyrolysis led to pores generation and, as summarized in Table 2, to SSA increase from 560 m^2/g to 596 m^2/g.

The SSA of the base formulation calculated using its composition and the SSA of each component in powder (i.e. 300–400 m^2/g for cellulose nanofibers [27], 1–7 m^2/g and chitosan [28] and graphene measured value given in Table 2) was of ca. 630 m^2/g. This SSA value indicates that materials blending and printing in the form of macroporous electrode leads to a decrease of SSA down to 560 m^2/g. The drop of 70 m^2/g in SSA was associated to a reduced accessibility of graphene pores due to the typical film forming ability of cellulose nanofibers /chitosan [29] and the formation of a barrier layer around graphene particles [30].

Nevertheless, cellulose/chitosan carbonization during pyrolysis improved pores accessibility and the undoped pyrolyzed electrode displayed a SSA of 593 m^2/g, i.e. only 5% lower than the theoretical one. The chronoamperometry of 3D pyrolyzed electrodes with different infill illustrated in Figure 4a shows that the largest faradic current was obtained with a theoretical infill rate of around 40%, i.e. 20 µA/mg (770 µA/cm^2) under air and 35 µA/mg (1361 µA/cm^2) under oxygen saturation conditions. As demonstrated in a previous study for 3D electrodes containing n-doped graphene [17], the current vs. infill ratio replotted from [17] (Figure 4b) shows that after a peak at 40% infill, the faradic current progressively decreased reaching lower values at 100% infill. This trend was interpreted as reflecting the progressive clogging of the macroporous structure, which led to a lower doping yield during pyrolysis, lower electrolyte wetting of electrode pores inducing a harder accessibility to the catalytic sites thus, a drop of the electrochemical activity. At 40% infill, the in-situ n-doping led to a ~2.6-fold increase of specific current with respect to 3D cathodes manufactured using Fe/n-doped graphene [17]. This substantial increase of the catalytic activity of pyrolyzed electrodes was associated to the increase in porosity and to the creation of catalytic sites on the electrode surface that can be easily reached by the electrolyte.

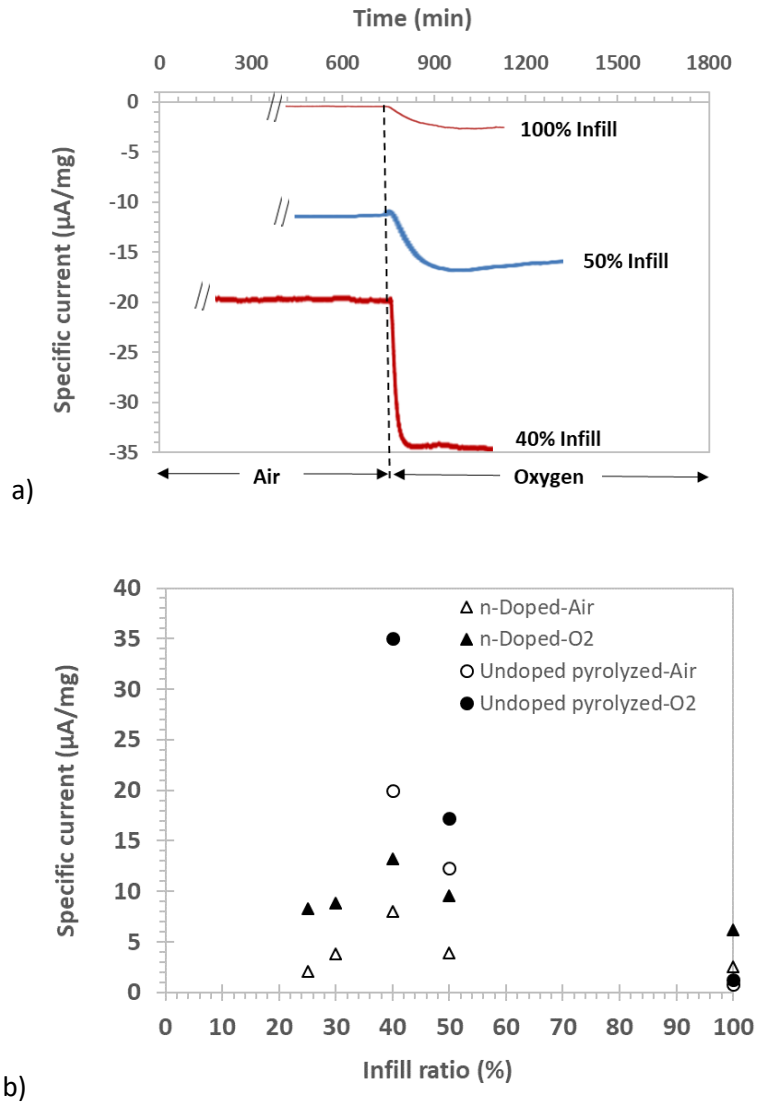

Fig. 4 Chronoamperometries at 100 mV. Vs. SCE in a physiological medium (pH = 7.4) of undoped pyrolyzed 3D cathodes with different infill under air and oxygen a). Pyrolyzed cathodes comparison with specific current generated by n-doped cathodes b). Specific current data of n-doped cathodes with 25, 30, 50 and 100% infill are replotted from [17]

In-situ doping of 3D electrodes allowed to go beyond the typical limitation of catalyst pre-mixing in the 3D printing ink, which induces a partial segregation of the catalyst in the bulk electrode with a subsequent drop of active sites in contact with the physiological medium used as electrolyte and of the overall electrochemical activity [17].

When compared to 2D biocathodes manufactured using similar composition and standard methods, 3D pyrolyzed cathodes displayed higher electrochemical activity delivering a specific current, which was 7- (i.e. from 5 to 35 µA/mg in O_2) and 5-fold the current delivered by electrodes manufactured by blade-coating [19] and powder compression [31], respectively. Despite the excellent electrochemical properties of pyrolyzed cathodes, carbon materials can have biocompatibility issues an induce severe inflammatory reactions after implantation [31]. Additional electrode encapsulation and in vivo test [17,31] are therefore necessary to assess the long-term biocompatibility of 3D abiotic cathodes developed in this study.

4 Conclusion

To conclude, chitosan, TOCNF, graphene nanoplatelets and Fe-GO have been used for the 3D printing of porous electrodes with different macroporosity. The subsequent in-situ n-doping of graphene by cathode's pyrolysis under ammoniac flux, led to the improvement of the electrode's electrochemical activity and specific surface area. Indeed, when compared to 3D cathodes elaborated using pre-doped Fe/n-G, pyrolyzed cathodes displayed high BET specific surface area (i.e. 596 m^2/g, close to the theoretical 630 m^2/g calculated for the blend of individual components) and the specific current under oxygen of reference electrodes with 40% infill rose from 13 µA/mg of the standard formulation to 35 µA/mg of the pyrolyzed one. 3D electrodes densification by increasing the volumetric infill to 50 and 100% led to a progressive decay of the electrochemical activity, which was associated with macropores clogging and a drop in the electrode surface available for in-situ doping and direct contact with the electrolyte. In-situ doped 3D cathodes delivered a specific current 5-7 and 2.5 times higher than homologues 2D and 3D electrodes manufactured using pre-doped Fe/n-G. This sound increase in specific current highlights in-situ n-doping as a promising manufacturing process for the fabrication of high current density 3D abiotic cathodes for biofuel cells.

Author Contributions

M. Ghodhbane: Conceptualization, Methodology, Investigation,
Formal analysis, Data curation, Writing – original draft.
D. Beneventi: Conceptualization, Methodology, Formal analysis, Visualization, Writing – original draft.
L. Dubois: Conceptualization, Methodology, Project administration, Writing – review & editing.
A. Zebda: Conceptualization, Methodology, Formal analysis, Writing – review & editing.
D. Chaussy: Conceptualization, Methodology, Formal analysis, Writing –review & editing.
N. Belgacem: Conceptualization, Methodology, Formal analysis, Supervision.

Conflicts of interest

The authors declare that they have no known competing financial interests or personal relationships that could have appeared to influence the work reported in this paper.

Acknowledgements

This work was supported by the National Research Agency, France (Implantable Abiotic Biofuel Cell – IMaBiC, ANR-16-CE19-0007) France, the "Laboratoire d'Excellence" Tec21 France, Region Auvergne Rhône Alpes SCUSI program 2018 (no. 187370) and Pack Amb Int'l 2019 (no. Pack Amb Int'l 2019).
The authors thank L. Cortella for the access to radiation facilities at ARC-Nucléart (CEA Grenoble).

References

1. Bao Y, Liu Y, Kuang Y, Fang D, Li T, (2020) 3D-printed highly deformable electrodes for flexible lithium ion batteries. *Energy Storage Materials* 33:55-61. https:// doi.org/ 10.1016/j.ensm.2020.07.010

2. Cao D, Xing Y, Tantratian K, Wang X (2019) 3D Printed High-Performance Lithium Metal Microbatteries Enabled by Nanocellulose. *Advanced Materials* 31(14):1807313. https://doi.org/10.1002/adma.201807313
3. Li J, Leu MC, Panat R, Park J (2017) A hybrid three-dimensionally structured electrode for lithium-ion batteries via 3D printing. *Materials & Design* 119:417-424. https://doi.org/10.1016/j.matdes.2017.01.088
4. Lyu Z, Jia Hao GL, Gu R, Pan Z (2020) 3D-printed electrodes for lithium metal batteries with high areal capacity and high-rate capability. *Energy Storage Materials* 24:336-342. https://doi.org/10.1016/j.ensm.2019.07.041
5. Shen K, Ding J, Yang S (2018) 3D Printing Quasi-Solid-State Asymmetric Micro-Supercapacitors with Ultrahigh Areal Energy Density. *Advanced Energy Materials* 8(20):1800408. https;//doi.org/10.1002/aenm.201800408
6. Idrees M, Ahmed S, Mohammed Z, Korivi NS, Rangari V (2020) 3D printed supercapacitor using porous carbon derived from packaging waste. *Additive Manufacturing* 36:101525. https://doi.org/10.1016/j.addma.2020.101525
7. Li X, Li H, Fan X, Shi X, Liang J (2020) 3D-Printed Stretchable Micro-Supercapacitor with Remarkable Areal Performance. *Advanced Energy Materials* 10(14):1903794. https://doi.org/10.1002/aenm.201903794
8. Wang Z, Zhang Q, Long S, Luo Y (2018) Three-Dimensional Printing of Polyaniline/Reduced Graphene Oxide Composite for High-Performance Planar Supercapacitor. *ACS Appl. Mater. Interfaces* 10(12):10437-10444. https://doi.org/10.1021/acsami.7b19635
9. Nesaei S, Song Y, Wang Y, Ruan X (2018) Micro additive manufacturing of glucose biosensors: A feasibility study. *Analytica Chimica Acta* 1043:142-149. https://doi.org/10.1016/j.aca.2018.09.012
10. Suresh RR, Lakshmanakumar M, Arockia Jayalatha JBB, et al. (2021) Fabrication of screen-printed electrodes: opportunities and challenges. J Mater Sci 56(15):8951-9006. https:/doi.org/10.1007/s10853-020-05499-1
11. Postiglione G, Natale G, Griffini G, Levi M, Turri D (2015) Conductive 3D microstructures by direct 3D printing of polymer/carbon nanotube nanocomposites via liquid deposition modelling. *Composites Part A: Applied Science and Manufacturing* 76:110-114. https://doi.org/10.1016/j.compositesa.2015.05.014
12. Foster CW, Down MP, Zhang Y, Ji X (2017) 3D Printed graphene-based energy storage devices. *Scientific Reports* 7(1), Art. nº 1. https://doi.org/10.1038/srep42233
13. Yao B, Chandrasekaran S, Zhang J, Xiao W, Qian F et al. (2019) Efficient 3D Printed Pseudocapacitive Electrodes with Ultrahigh MnO_2 Loading. *Joule* 3(2):459-470. https://doi.org/10.1016/j.joule.2018.09.020
14. Gulzar U, Glynn C, O'Dwyer C (2020) Additive manufacturing for energy storage: Methods, designs and material selection for customizable 3D printed batteries and supercapacitors. *Current Opinion in Electrochemistry* 20:46-53. https://doi.org/10.1016/j.coelec.2020.02.009

15. Sun C, Liu S, Shi X, Lai C, Liang J, Chen Y (2020) 3D printing nanocomposite gel-based thick electrode enabling both high areal capacity and rate performance for lithium-ion battery. *Chemical Engineering Journal* 381:122641. https://doi.org/10.1016/j.cej.2019.122641
16. Wang J, Sun Q, Gao X, Wang C (2018) Toward High Areal Energy and Power Density Electrode for Li-Ion Batteries via Optimized 3D Printing Approach. *ACS Appl. Mater. Interfaces* 10(46):39794-39801. https://doi.org/10.1021/acsami.8b14797
17. Ghodhbane M, Beneventi D, Zebda A, Dubois L et al. (2023) 3D printed cathodes for implantable abiotic biofuel cells. *Journal of Power Sources*, 580:233356. https://doi.org/10.1016/j.jpowsour.2023.233356
18. Meyer V, Tapin-Lingua S, Da Silva Perez D, Arndt T, Kautto J (2012) Technical opportunities and economic challenges to produce nanofibrillated cellulos in pilot scale: NFC delivery for applications in demonstrations trials. In: Proceed. SUNPAP EU Project—Final Conference, 19–20 June, 2012, Milan, Italy. https://cordis.europa.eu/project/id/228802/reporting
19. Ghodhbane M, Menassol G, Beneventi D, Chaussy D, Dubois L, Zebda A, Belgacem MN (2023) Flexible doctor blade-coated abiotic cathodes for implantable glucose/oxygen biofuel cells, RSC Advances 13:3877–3889. https:/doi.org/10.1039/d2ra03471a
20. Li X, Wang H, Robinson JT, Sanchez H, Diankov G, Dai H (2009) Simultaneous Nitrogen Doping and Reduction of Graphene Oxide. Journal of the American Chemical Society 131(43):15939-15944. https://doi.org/10.1021/ja907098f
21. Rhim Y-R, Zhang D, Fairbrother DH, Wepasnick KA, Livi KJ, Bodnar RJ, Nagle DC (2010) Changes in electrical and microstructural properties of microcrystalline cellulose as function of carbonization temperature. Carbon 48(4):1012-1024. https://doi.org/10.1016/j.carbon.2009.11.020
22. Zhao W, Liu S, Yin M, He Z, Bi D (2023) Co-pyrolysis of cellulose with urea and chitosan to produce nitrogen-containing compounds and nitrogen-doped biochar: Product distribution characteristics and reaction path analysis. Journal of Analytical and Applied Pyrolysis 169:105795. https://doi.org/10.1016/j.jaap.2022.105795
23. Liu W, Speranza G (2021) Tuning the oxygen content of ceduced graphene oxide and effects on its properties. ACS Omega 6:6195−6205. https://doi.org/10.1021%2Facsomega.0c05578
24. Ganesan A, Shaijumon MM, (2016) Activated graphene-derived porous carbon with exceptional gas adsorption properties. Microporous and Mesoporous Materials 220: 21-27. https://doi.org/10.1016/j.micromeso.2015.08.021
25. Thommes M, Cychosz KA (2014) Physical adsorption characterization of nanoporous materials: progress and challenges. Adsorption 20:233–250. https://doi-org.sid2nomade-1.grenet.fr/10.1007/s10450-014-9606-z
26. Shao Y, Guizani C, Grosseau P, Chaussy D, Beneventi D (2017) Thermal characterization and kinetic analysis of microfibrillated cellulose/lignosulfonate blends. *Journal of Analytical and Applied Pyrolysis* 124:25-34. https://doi.org/10.1016/j.jaap.2017.03.001
27. Henriksson MG, Lindström ME (2016) Specific surface area increase during cellulose nanofiber manufacturing related to energy input. *BioResources* 11(3):7124-7132. https://doi.org/10.15376/biores.11.3.7124-7132

28. Luo W, Bai Z, Zhu Y (2018) Fast removal of Co(II) from aqueous solution using porous carboxymethyl chitosan beads and its adsorption mechanism. R*SC Advances* 8:13370-13387. https://doi.org/10.1039/C7RA13064C
29. Soni B, Hassan EB, Schilling MW, Mahmoud B (2016) Transparent bionanocomposite films based on chitosan and TEMPO-oxidized cellulose nanofibers with enhanced mechanical and barrier properties. Carbohydrate Polymers 151:779-789. https://doi.org/10.1016/j.carbpol.2016.06.022
30. Hsan N, Dutta PK, Kumar S, Bera R, Das N (2019) Chitosan grafted graphene oxide aerogel: Synthesis, characterization and carbon dioxide capture study. International Journal of Biological Macromolecules 125:300-306. https://doi.org/10.1016/j.ijbiomac.2018.12.071
31. Penven G, Menassol G, Alcaraz J-P, Boucher F, Thélu J et al. (2020) The biocompatibility of biofuel cells operating inside the body. *Biochemical Society Transactions* 48(3):867-879. https://doi.org/10.1042/bst20190618